# Carbon cycling within the sulfate-methane-transition-zone in marine sediments from the Ulleung Basin

Wei-Li Hong[1*], Marta E. Torres[1], Ji-Hoon Kim[2], Jiyoung Choi[2,3], and Jang-Jun Bahk[2]

[1] *College of Earth Oceanic and Atmospheric Sciences, Oregon State University, Corvallis, Oregon, United States*

[2] *Petroleum and Marine Resource, Korea Institute of Geosciences and Mineral Resources, Republic of Korea*

[3] *Division of Marine Environment & Bioscience, Korea Maritime University, 1 Dongsam-dong, Yeongdo-gu, Busan, 606-791, Republic of Korea*

*Corresponding Author: Phone: +1 541-737-2467; Fax: +1 541-737-2064

E-mail: whong@coas.oregonstate.edu

## Abstract

The significance of the various carbon cycling pathways in driving the sharp sulfate methane transition (SMTZ) observed at many locations on continental margins is still a topic of debate. Unraveling these processes is important to our understanding of the carbon cycle in general and to evaluate whether the location of this front can be used to infer present and past methane fluxes from deep reservoirs (*e.g.,* gas hydrate). Here we report the pore water data from the second Ulleung Basin Gas Hydrate Expedition (UBGH2) and on the results of a box model that balances solute fluxes among different carbon pools and satisfies the observed isotopic signatures. Our analysis identifies a secondary methanogenesis pathway within the SMTZ, whereby 25 to 35% of the dissolved inorganic carbon (DIC) produced by the anaerobic oxidation of methane (AOM) is consumed by $CO_2$ reduction (CR). To balance this DIC consumption, a comparable rate of organic matter degradation becomes necessary, which in turn consumes a significant amount of sulfate. The fraction of sulfate consumed by AOM ranges from 70 to 90%. Whereas a simple mass balance would suggest a one to one relationship between sulfate and methane fluxes; our isotopic considerations show that methane flux estimates based solely on sulfate data may be in error by as much as 30%. Furthermore, the carbon cycling within the SMTZ is fueled by a significant contribution (10-40%) of methane produced by organic matter degradation just below the SMTZ. Therefore AOM rates cannot necessarily be used to infer methane contributions from gas hydrate reservoirs that may lay tens to hundreds of meters below the SMTZ.

*Keywords: anaerobic oxidation of methane, $CO_2$ reduction, sulfate-methane-transition-zone, cold seep environment*

# 1. Introduction

The sulfate methane transition zone (SMTZ) along continental margins, where sulfate is almost depleted and methane concentration starts to dramatically increase (Figure 1), is usually no deeper than a few to tens of meters. We have a good first order understanding of the reactions driving this front; however, the various carbon cycle pathways involved, and the relative fraction of sulfate consumed by these reactions is still being debated. Using data from sediment cores taken off Namibia and assuming there was no organoclastic sulfate reduction at the sediment surface, Niewöhner et al. (1998) suggested that the sulfate flux in this region can be fully explained by anaerobic oxidation of methane (AOM). On the other hand, down-core sulfate reduction rate measurements were used by Fossing et al. (2000) to demonstrate that more than 60% of the sulfate reduction can occur within the first meter of the sediments due to fast organic matter degradation. For the Black Sea, Jørgensen et al. (2001) showed that sulfate profile remained unaffected by organoclastic sulfate reduction because in this area sulfate diffuses rapidly into surface sediments, whereas sulfate is replenished only very slowly at the SMTZ depth. These data suggest that in diffusive systems, sulfate profiles may be fully dictated by AOM and not by organoclastic sulfate reduction, even if there was a significant component of organoclastic sulfate reduction in the shallowest sediments.

These results are significant because, if the depth of the SMTZ were to scale inversely with the strength of an upward diffusive methane flux, sulfate can be used as a proxy for the methane supply from the gas hydrate reservoirs, as postulated by several investigators (Borowski et al., 1996, 1999; Niewöhner et al., 1998; Dickens, 2001; Lin et al., 2006; Yang et al., 2008; Chuang et al., 2006, 2010). However, such inference is based on two simplified assumptions: 1) sulfate is dominantly consumed by methane through AOM and 2) all the methane consumed by AOM comes from gas hydrate dissociation. The first assumption may be undermined if there is a significant contribution of sulfate reduction fueled by organic matter degradation above or within the SMTZ. The second assumption may also be problematic, since a zone of methane generation by microbial activity has been shown to occur just below the SMTZ (Oremland et al., 1982; Claypool et al., 2006; Colwell et al., 2008). To account for

this shallow zone of methane generation, we incorporate it into our model, and designate our box as an expanded sulfate methane transition zone (ESMTZ) (Figure 1). The upper boundary of this box is demarked by the sharp transition in the sulfate and methane profiles, and the lower boundary is conceptually defined to include the methanogenesis zone just below the depth where sulfate is exhausted.

Here we report on pore water profiles for the upper 30 m at five sites drilled in the Ulleung Basin offshore Korea, and present a complete mass balance approach that includes concentrations, isotopes and fluxes of various metabolites from SMTZ or ESMTZ (Figure 1). Our primary conclusion is that, while AOM may consume much of the sulfate in this basin, other pathways that modify the DIC concentration –namely, reduction of POC, and shallow methanogenesis- are important, and need to be quantified. We argue that the methane produced locally by converting DIC from AOM into methane (secondary methanogenesis) and from organic carbon diagenesis immediately below SMTZ need to be considered in order to achieve a carbon isotopic mass balance across the SMTZ. These shallow methane sources, both distinct in the isotopic composition of the substrate, need to be considered to fully characterize carbon cycle budgets and in the assessment of methane contribution from gas hydrate reservoirs based on sulfate gradients.

## 2. Study area and sediment properties

The Ulleung Basin, one of the three main basins in the East Sea, is bounded by the steep continental slope of the Korean Peninsula to the west and the Korean Plateau to the north (Figure 2A). This area harbors a thick (4 km) sediment section characterized by extensive turbidite and mass transport deposits, with moderate total organic matter content (~1-4%, Kim et al., 2007 and Table 1). Gas hydrates have been recovered from this margin, and hydrocarbon analyses point to a biogenic source for the methane in these deposits (Bahk et al., 2009; Chun et al., 2011; Kim et al., 2011, 2012).

Here we focus on five sites (UBGH2-1_1, 2-2_1, 2-5, 2-6, and 2-10) drilled during the second Ulleung Basin Gas Hydrate Expedition (UBGH2) in 2010 (Figure 2B).

The depth penetrated by these sites ranges from 230 to 360 meters below seafloor (mbsf). The depth of bottom simulating reflector (BSR), depth of gas hydrate first appearance, and average content of particulate organic carbon (POC) content, have been reported by the UBGH2 Scientists (2010), and are included in Table 1. The depth of the BSR is shallower than 190 meters at all sites. Gas hydrate in these sites was first observed at 71 to 153 mbsf. POC content ranges from less than 0.1% to 4%, with an average of ~1.5%.

Onboard porosity measurements at these sites show that they follow the classic equation for depth-dependent porosity (Boudreau, 1997):

$$\phi(z) = \phi_f + (\phi_0 - \phi_f)\exp(\gamma z) \quad (1)$$

where $\phi_f$ and $\phi_0$ are porosity at great depth and at the water-sediment interface, respectively. $\gamma$ is an empirical constant, which can be obtained from data fitting and $z$ is the depth in the sediments. The measured porosity (UBGH2 Scientists, 2010) and trends used to fit those measurements are shown in Figure 3. Parameters used to fit the observations according to Eq.(1) are listed in Table 2. These fitted trends will be used for porosity estimation in our box model.

# 3. Analytical method and results

## 3.1 Sample collection

Pore water, gas, gas hydrate and sediment samples were collected from all the drilled sites following the protocols detailed in UBGH2 Scientists (2010). Pore water was extracted from whole round sediment samples (5-20 cm length) collected immediately after retrieval of the cores. Following extrusion from the core liner, the surface of the sediment sample was carefully scraped with a clean spatula or clean ceramic knife to avoid any contamination with drilling fluid (ambient surface seawater). Pore water was extracted from the clean sediments using titanium squeezer, modified after the stainless steel squeezer of Manheim and Sayles (1974), and a laboratory Carver

hydraulic press (< 20 MPa). Pore water was filtered through a Whatman paper and a 0.20 µm disposable polytetrafluoroethylene in-line filter, and collected in HCl prewashed syringes. Aliquots were transferred into HCl prewashed high density polyethylene vials for shipboard analyses of major and minor ions. Subsamples for isotopic analyses of the dissolved inorganic carbon (DIC) were collected in 2 ml septum screw-lid glass vials and preserved with $HgCl_2$.

Void gases in the core were sampled by piercing the liner and allowing gas to expand into a 60 ml syringe connected to the penetration tool. The gas sample was then transferred to a 50 ml serum glass vial which was pre-filled with saturated NaCl solution. For headspace gas analyses, a 3 ml sediment sample was taken with a 5 ml cut-off plastic syringe from the freshly exposed end of each core section, and extruded into a 30 ml serum glass vial. Following the method described in Riedel et al. (2006), 2 ml of saturated NaCl was added to each vial, which was then sealed with a 10 mm-thick septum and a metal crimp cap to preserve the samples.

### 3.2 Analytical approaches

Sulfate and alkalinity were measured onboard. The first 5 ml of pore water was immediately subsampled for pH and alkalinity determinations using a pH electrode and a Gran titration with a Metrohm autotitrator. The precision of the alkalinity titrations was monitored by repeated analysis of International Association for the Physical Sciences of the Ocean (IAPSO) standard seawater, and was less than 2%. Sulfate was analyzed by ion chromatography (Dionex ICS-2100 IC) using 0.2 ml samples diluted with 5.8 ml of Milli-Q water. At the beginning and the end of each run, several different dilutions of IAPSO standard seawater were analyzed as a quality control and to determine accuracy. IAPSO standard seawater was analyzed after every seven samples as a check for instrumental drift and to calculate analytical precision. Precision for the sulfate analyses was better than 0.8%, and average accuracy was better than 1.5%.

Immediately after samples were collected, concentration of methane, ethane, propane, and $CO_2$ in the head space and void gas samples were measured onboard by gas chromatography (GC; Agilent 3000A Micro GC) with a thermal conductivity detector

(TCD) and two independent columns: PLOT-U (8 m long and 0.32 mm inner diameter) for $C_1$-$C_4$ hydrocarbons and MolSieve 5A Plot (10 m long and 0.32 mm inner diameter) for $O_2$, $N_2$, $CO_2$ and CO. The temperature of the injector and the Plot-U column is stabilized at 90 $^oC$ while the temperature for the MolSieve 5A Plot is 105 $^oC$. Helium is chosen as carrier gas and column flow rate is 2.2 ml/min. The accuracy of $CH_4$ and $CO_2$ analysis, determined by repeated measurements of 1% standard gas, is better than 4 % and 6%, respectively. Since both headspace gas and void gas samples suffered from severe degassing during core recovery, it is impossible to precisely determine the in-situ gas concentration.

The isotopic composition of DIC in pore water was analyzed with a Finnigan DELTA-Plus mass spectrometer using a Gas-Bench II automated sampler at Oregon State University, as described in Torres et al. (2005). The precision and accuracy are better than ±0.15‰ and ±0.07‰, respectively, based on the multiple standard measurements. The stable carbon isotope of methane ($\delta^{13}C_{CH4}$) was measured using an isotope ratio-monitoring gas chromatography/mass spectrometer in Isotech, Champaign, IL. The reproducibility was ±0.1‰. The stable carbon isotope values for DIC and methane are reported in the conventional δ notation in permil (‰) relative to V-PDB.

### 3.3 Analytical results

The concentration profiles of the parameters required for our box model are illustrated in Figure 4 and listed in Table 3. Data and the detailed calculations can be found in the supplementary material online. The depth of the SMTZ was defined by the sulfate and methane profiles at each site. Since this study only examines the carbon cycling around the depth of the SMTZ, we only show data for the upper 30 mbsf. We did not differentiate among the various dissolved carbonate species (bicarbonate, carbonate, and $CO_{2(g)}$) but treat them as a single DIC (dissolved inorganic carbon) pool. Alkalinity can reasonably represent DIC concentration within the pH range of our samples (7.3-7.8). Therefore, alkalinity is used as synonymous with DIC throughout this paper. The alkalinity and calcium profiles show a distinct change in their concentration gradient across the depth of the SMTZ, indicating that the bicarbonate

produced by AOM increases alkalinity and consumes calcium through authigenic carbonate precipitation. Abnormally high alkalinity around the SMTZ was explained by Kim et al. (2011) as an indication of DIC leaking from a deep methanogenesis zone; this observation suggests that organic matter degradation by methanogenesis is an important component of the carbon cycling in the Ulleung Basin. The carbon isotopic profiles of methane and DIC, display minimum values around the SMTZ, reflecting the carbon pathways between the methane and DIC pools through AOM and CR, as previously suggested by Borowski et al. (1997) for Blake Ridge sediments.

## 4. Box model framework

We constructed a model that encompasses the SMTZ and the methanogenesis zone immediately below the depth of sulfate depletion; in a zone we designate ESMTZ. It includes 2 solid phases (organic matter and authigenic carbonate) and 3 dissolved components (sulfate, methane, and alkalinity) (Figure 5). All symbols used are listed in the Appendix. For the three dissolved components in Figure 5, we constructed a mass balance between input and output rates and fluxes, which includes transport (grey arrows) and reaction terms (red, orange, blue, purple, and green arrows). All components are linked via five reactions with a different degree of isotopic fractionation, which is parameterized as:

$$\alpha = \frac{r_r}{r_p} \quad (2)$$

where $r_r$ and $r_p$ are the isotopic ratios ($^{13}C/^{12}C$) of the reactant and product.

The five reactions under consideration are:

POC sulfate reduction (POCSR):

$$CH_2O + \frac{1}{2}SO_4^{-2} \rightarrow \frac{1}{2}H_2S + HCO_3^- \quad \delta^{13}C_{CH2O}=-23‰, \ \alpha_{POCSR} \cong 1 \quad (3)$$

Calcium carbonate precipitation (CP):

$$Ca^{+2} + CO_3^{-2} \rightarrow CaCO_3 \quad \delta^{13}C_{DIC}=\text{varies}, \ \alpha_{CP} \cong 1 \quad (4)$$

Anaerobic oxidation of methane (AOM):

$$CH_4 + SO_4^{-2} \rightarrow HS^- + HCO_3^- \quad \delta^{13}C_{CH4}=\text{varies}, \ 1.004 < \alpha_{AOM} < 1.03 \quad (5)$$

Secondary methanogenesis or $CO_2$ reduction (CR)

$$CO_2 + 4H_2 \rightarrow CH_4 + 2H_2O \quad \delta^{13}C_{DIC}, {}^{13}C_{CH4} =\text{varies}, \ 1.01 < \alpha_{CR} < 1.095 \quad (6)$$

Methanogenesis (ME)

$$CH_2O \rightarrow \frac{1}{2}CH_4 + \frac{1}{2}CO_2 \quad \delta^{13}C_{DIC}, {}^{13}C_{CH4} =\text{varies}, \delta^{13}C_{CH2O}=-23‰,$$

$$1.01 < \alpha_{ME} < 1.095 \quad (7)$$

The isotopic fractionation factors listed here are from Whiticar (1999). Organic matter degradation via sulfate (POCSR, Eq. (3)) usually occurs well above the SMTZ (e.g., in the first tens centimeters below sediment-water interface as shown in Fossing et al. (2000)). Although POCSR does not occur within the SMTZ, it consumes a portion of sulfate supply from the seafloor and, therefore, decreases the flux of sulfate into the SMTZ. POCSR is thus expressed as the portion of sulfate flux that does not enter the SMTZ in our box model. AOM (Eq. (5)) that consumes both sulfate and methane in the SMTZ produces DIC and induces precipitation of calcium carbonate (Eq. (4)), which consumes most of the calcium flux from seafloor.

The first three reactions discussed above (Eqs. (3) to (5)) has been well accepted among literature (*e.g.,* Kim et al., 2007 and Chatterjee et al., 2011). However, Eqs. (6) and (7) are typically not considered in carbon cycling studies around the SMTZ, even though there are several studies showing that the rate of microbial methanogenesis peaks immediately below the SMTZ (*e.g.,* Oremland et al., 1982; Claypool et al., 2006; Colwell et al., 2008). Secondary methanogenesis or CR, is specified in our model as the reaction utilizes $CO_2$ produced from AOM. For methanogenesis (ME), the primary substrate is organic carbon. Whereas this metabolic process involves several steps (*e.g.*, production of $CO_2$ and hydrogen gas; and carbonate reduction to methane), for the purpose of the model it is described by reaction (7). These two reactions that generate methane (CR and ME) are defined in terms of their carbon

sources: the DIC produced by ME comes directly from organic matter decomposition while the DIC utilized by CR is produced by AOM and it is not directly linked to organic matter degradation.

Within the ESMTZ (defined to include the zone of methanogenesis below the SMTZ, Figure 1), the following three equations are used to describe the mass balance for sulfate, DIC, and methane:

$$F_{SO4.in}=F_{SO4.out}+R_{POCSR\text{-}S}+R_{AOM} \quad (8)$$

$$F_{DIC.in}+R_{ME\text{-}DIC}+R_{POCSR\text{-}C}+R_{AOM}=F_{DIC.out}+R_{CR}+R_{CP} \quad (9)$$

$$F_{CH4.in}+R_{CR}+R_{ME\text{-}CH4}=F_{CH4.out}+R_{AOM} \quad (10)$$

where "F" denotes flux, "R" denotes reaction rate, and *in* and *out* indicate the flux direction relative to the ESMTZ. $R_{POCSR\text{-}S}$ and $R_{POCSR\text{-}C}$ are the rates of sulfate consumption and DIC production through POCSR. They relate to each other according to the stoichiometry in Eq. (3) (*i.e.*, $R_{POCSR\text{-}C}=2\times R_{POCSR\text{-}S}$). $R_{ME\text{-}DIC}$ and $R_{ME\text{-}CH4}$ are rates of ME in terms of DIC and methane production. Both of these rates are half of the ME rate (*i.e.*, $R_{ME}=2\times R_{ME\text{-}DIC}=2\times R_{ME\text{-}CH4}$) followed the stoichiometry in Eq. (7). These fluxes and rate terms are illustrated in Figure 4 and 5. In our following calculations and discussion, we assume that both sulfate and methane are fully consumed within the ESMTZ, so that the values for $F_{SO4.out}$ and $F_{CH4.out}$ are negligible and can be ignored in Eq.(8) and (10). $F_{CH4.in}$ denotes the flux of methane that comes from outside the box (Figure 1) and carries a distinct isotopic signature that is not related to any reaction considered in our model frame.

### 4.1 Transport terms

This study focuses on sites with diffusion-dominated concentration profiles (Figure 4), and where no sign of advective flow was observed emerging from seafloor or in geophysical surveys (UBGH2 Scientists, 2010). By assuming a diffusion-dominated system under steady state, we can quantify the magnitude of the fluxes $F_{in}$ and $F_{out}$ with Fick's law:

$$F = -D\frac{\Delta(\phi C)}{\Delta z} \quad (11)$$

Porosity information is given in Figure 3 and Table 2. Tortuosity-corrected diffusion coefficients (D) for sulfate, calcium, and DIC are derived from the relationships in Boudreau (1997) assuming a constant temperature in the sediments of 4°C. The concentration gradients ($\frac{\Delta(\phi C)}{\Delta z}$) are calculated from individual profiles and are used to calculate $F_{in}$ and $F_{out}$. Since most of the gradients in our sites are linear, we apply a simple 1st order linear regression to calculate each gradient (Table 3).

To satisfy isotopic mass balance considerations, it is necessary to calculate the transport of both the heavy and light carbon (*i.e.,* $^{13}C$ and $^{12}C$) by $CH_4$ and DIC. In combination with measured isotopic ratios, this information is used to infer the concentration profiles for $^{12}C_{DIC}$ and $^{13}C_{DIC}$ as follows:

$$^{12}C_{DIC} = \frac{C_T}{(1+r_{DIC})} \qquad (12)$$
$$^{13}C_{DIC} = C_T - {}^{12}C_{DIC}$$

where $C_T$ is the total concentration (*i.e.,* alkalinity in Figure 4) and $r_{DIC}$ is the concentration ratio of heavy to light carbon ($^{13}C/^{12}C$) from its isotopic value:

$$r_{DIC} = (\frac{\delta^{13}C_{DIC}}{1000} + 1) \times r_{std} \qquad (13)$$

where $r_{std}$ is the ratio for V-PDB standard (0.0112372).

A migration-induced isotopic fractionation is related to the mass ratio of the two isotopes (Zeebe and Wolf-Gladrow, 2001). However, since such fractionation is much smaller than the fractionation from other reactions (diffusion coefficients of $^{13}CO_2$ is

only 0.7-0.87 ‰ smaller than it for $^{12}CO_2$; O'Leary, 1984 and Jähne and Dietrich, 1987), we have neglected it in our calculation.

### 4.2 Reaction terms

The isotopic fractionation for each of the five reactions considered here (Eqs. (3) to (7)), is fundamental to our understanding of processes occurring within the SMTZ. The isotopic effect ($\alpha$) for a steady-state one-step reaction may be expressed in terms of the rate constant of the heavy ($k^H$) and light ($k^L$) isotopes (Rees, 1973):

$$\alpha = \frac{k^L}{k^H} \qquad (14)$$

From Eqs. (2) and (14), we can then formulate the reaction rates for all light and heavy isotopes. For *light* carbon (*i.e.,* $^{12}C$), reactions are formulated as follow:

$$^{12}R_{POCSR\text{-}S} = \phi\left(\frac{1}{2} f R_{OM}\right) \qquad (15)$$

$$^{12}R_{POCSR\text{-}C} = \phi\left(f R_{OM}\right) \qquad (16)$$

$$^{12}R_{ME\text{-}DIC} = \phi(1-f)\frac{1}{2} R_{OM} \qquad (17)$$

$$^{12}R_{ME\text{-}CH4} = \phi(1-f)\frac{1}{2} R_{OM} \qquad (18)$$

$$^{12}R_{AOM} = F_{SO4.in} - \phi\frac{1}{2} f R_{OM} \qquad (19)$$

$$^{12}R_{CP} = F_{Ca} \qquad (20)$$

$$^{12}R_{CR} = b\,^{12}R_{AOM} \qquad (21)$$

where $R_{OM}$ is the rate of organic matter degradation through both POCSR and ME (*i.e.,* $R_{OM}=R_{ME}+R_{POCSR\text{-}C}$), $f$ is the fraction of organic matter being utilized by POCSR. Stoichiometric considerations are included by the 0.5 multiplier in Eq. (15)

(*i.e.,* every mole of organic matter consumed by sulfate is equivalent to 0.5 moles of sulfate) and the 0.5 multiplier in Eq. (17) and (18) (*i.e.,* every mole of organic matter consumed by methanogenesis produces 0.5 moles each of DIC and $CH_4$). To describe the production of methane through CR from the pool of DIC generated by AOM (Borowski et al., 1997), we assume the rate of CR is proportional to AOM rate within the SMTZ (Eq. (21)). Based on this definition, *b* in Eq. (21) must range from 0 to 1.

For the *heavy* carbon (*i.e.,* $^{13}C$), we apply the following reaction rate expressions

$$^{13}R_{POCSR\text{-}C} = \phi(fR_{OM})r_{OM} \qquad (22)$$

$$^{13}R_{ME\text{-}DIC} = \phi(1-f)\frac{1}{2}R_{OM}r_{DIC-bot} \qquad (23)$$

$$^{13}R_{ME\text{-}CH4} = \phi(1-f)\frac{1}{2}R_{OM}r_{CH4-bot} \qquad (24)$$

$$^{13}R_{AOM} = (F_{SO4.in} - \phi\frac{1}{2}fR_{OM})\frac{r_{CH_4-SMTZ}}{\alpha_{AOM}} \qquad (25)$$

$$^{13}R_{CP} = F_{Ca} \times r_{DIC-SMTZ} \qquad (26)$$

$$^{13}R_{CR} = b^{13}R_{AOM} \times \frac{1}{\alpha_{CR}} \qquad (27)$$

where *r* is the $^{13}C$ to $^{12}C$ ratio of organic matter ($r_{OM}$), DIC, and $CH_4$ at the *SMTZ* ($r_{CH_4-SMTZ}$ and $r_{DIC-SMTZ}$) or bottom of the core ($r_{CH_4-bot}$ and $r_{DIC-bot}$) which can be calculated from the isotopic signature listed in Table 3. $\alpha_{AOM}$ is the fractionation factor of AOM, which we will calculate from the box model. $\alpha_{CR}$ is the isotopic fractionation of CR and ME. This value is estimated from the isotopic signature of DIC and $CH_4$ at the core bottom ($\alpha_{CR}=1+(\delta^{13}C_{DIC\text{-}bot}-\delta^{13}C_{CH4\text{-}bot})\times 1000$) for each site (Table 3). Detail calculation of the box model can be found from the supplementary material.

### 4.3 Assessment of the error associated with flux estimates

In our box model, reaction rates are always linked to the flux of dissolved species. Therefore, to estimate the errors in our model, we need to quantify the potential errors from our flux estimates; which fall within two general categories. The first include uncertainties associated with parameters such as porosity and tortuosity, which will have the same degree of influence on all fluxes at a given site. This type of error will only affect the absolute but not the relative magnitude of the fluxes, and since most of our discussion relies on the relative magnitude of the fluxes, these uncertainties do not directly impact our discussion.

The second type of error, which arises during the calculation of gradient from each of the chemical species, will affect both the absolute and relative magnitude of the fluxes and hence directly affect our conclusions. The error on our flux estimates is the sum of the error associated with fitting the concentration and isotopic profiles to the data, plus the standard error of the regression slope. Fitting of concentration profiles for sulfate and calcium fluxes is not necessary, thus for these species the error of the flux estimates arises solely from the standard error of regression line, and is usually smaller than 5% (Table 4). Fitting of the concentration and isotopic profiles of DIC based on insufficient data, is responsible for most of the error associated with the DIC flux estimates, which range from 6.2 to 20.3% while, in most cases, around 10 to 15%. The error of flux estimation may potentially increase the uncertainties of our rate estimation. Errors of different fluxes at different sites are summarized in Table 4. Detailed calculation of the errors is given in the supplementary material.

# 5. Model evaluation

To best illustrate the relative significance of each reaction involving carbon cycling at the ESMTZ, we run our box model on 4 different scenarios, as described below.

*Case1: Anaerobic oxidation of methane (AOM) as the only reaction*

In this first scenario (Figure 5A), we assumed that AOM is the *ONLY* reaction responsible for sulfate consumption and all methane for AOM is supported by upward diffusion of methane from below the SMTZ (*i.e.,* no reactions generate methane

within the SMTZ). Eq. (9) is modified and applied to both carbon isotopes, such that the relevant fluxes are estimated by:

$$F_{SO4.in}=R_{AOM} \qquad (28)$$

$$^{12}F_{DIC.in}+{}^{12}R_{AOM}={}^{12}F_{DIC.out}+{}^{12}R_{CP} \qquad (29)$$

$$^{13}F_{DIC.in}+{}^{13}R_{AOM}={}^{13}F_{DIC.out}+{}^{13}R_{CP} \qquad (30)$$

and Eq. (19) and (25) are modified to fit our assumption that sulfate is fully consumed by AOM:

$$^{12}R_{AOM}=F_{SO4.in} \qquad (31)$$

$$^{13}R_{AOM}=F_{SO4.in}\times\frac{r_{CH_4-SMTZ}}{\alpha_{AOM}} \qquad (32)$$

Eqs. (31) and (32) can be plugged into Eqs. (29) and (30), respectively. The $\alpha_{AOM}$ is the only remaining unknown in this set of equations. Using this approach and the data available for Site UBGH2-1_1, the $\alpha_{AOM}$ generated from this assumption is 0.934. Similar values for $\alpha<1$ were obtained for all sites (Figure 6). Both experimental and field data have shown that $\alpha_{AOM}$ is always slightly larger than 1 and ranges from 1.004 to 1.030 (Whiticar, 1999) due to the preferential utilization of light carbon during this microbial-mediated reaction. The results of our Case 1 scenario demonstrate that AOM alone is not sufficient to explain the isotopic composition of DIC and methane observed at the SMTZ.

Snyder et al. (2007) and Wehrmann et al. (2011) performed a similar calculation but did not include carbon isotopic considerations. Since they can fully satisfy Eq. (29) by their approaches, these authors concluded that AOM is the dominant reaction consuming sulfate. However, by including an isotopic mass balance we show the need to include other reactions, and argue that only balancing the fluxes of the total carbon does not provide sufficient evidence to conclude that AOM is the only reaction that needs consideration.

*Case2: Anaerobic oxidation of methane (AOM) and particulate organic carbon sulfate reduction (POCSR)*

Here our box model is formulated as:

$$F_{SO4.in}=R_{POCSR\text{-}S}+R_{AOM} \quad (33)$$

$$^{12}F_{DIC.in}+^{12}R_{POCSR\text{-}C}+^{12}R_{AOM}=^{12}F_{DIC.out}+^{12}R_{CP} \quad (34)$$

$$^{13}F_{DIC.in}+^{13}R_{POCSR\text{-}C}+^{13}R_{AOM}=^{13}F_{DIC.out}+^{13}R_{CP} \quad (35)$$

In this scenario (Figure 5B), organic matter is allowed to react with sulfate only (*i.e.,* $f$=1). $^{12}R_{POCSR\text{-}C}$ and $^{12}R_{AOM}$ can be solved from Eqs. (33) and (34) (assuming $^{12}R_{POCSR\text{-}C}=2\times R_{POCSR\text{-}S}$ and $^{12}R_{AOM}=R_{AOM}$). By plugging Eqs. (22) and (25) into Eq. (35), we can then estimate the isotopic fractionation for AOM ($\alpha_{AOM}$), which yields a value of 0.941 for Site UBGH2-1_1 (and similar values for other sites). Although this value is slightly larger than that by Case 1, it is still notably smaller than 1, demonstrating that the isotopic mass balance is not satisfied under the Case 2 scenario (Figure 6). The small $\alpha_{AOM}$ from Case 1 and 2 suggests that consumption of isotopically light DIC is required to fulfill the mass balance. Such sign suggests consumption of DIC through CR and leads us to the next case.

*Case3: Anaerobic oxidation of methane (AOM), particulate organic carbon sulfate reduction (POCSR) and secondary methanogenesis by $CO_2$ reduction (CR).*

By including in our methane sources the recycling of the DIC generated by AOM via $CO_2$ reduction (CR in Figure 5C), we now expand the conventional SMTZ to include the region of methanogenesis in our ESMTZ and have 4 unknowns: $R_{OM}$, $R_{AOM}$, $^{12}R_{CR,}$ and the fractionation factors of AOM ($\alpha_{AOM}$). In order to uniquely solve this set of equations, we need another constraint, which comes from the mass balance equations for methane. The equation set becomes:

$$F_{SO4.in}=R_{POCSR\text{-}S}+R_{AOM} \quad (36)$$

$$^{12}F_{DIC.in}+^{12}R_{POCSR\text{-}C}+^{12}R_{AOM}=^{12}F_{DIC.out}+^{12}R_{CR}+^{12}R_{CP} \quad (37)$$

$$^{13}F_{DIC.in}+^{13}R_{POCSR\text{-}C}+^{13}R_{AOM}=^{13}F_{DIC.out}+^{13}R_{CR}+^{13}R_{CP} \quad (38)$$

$$^{12}F_{CH4.in}+^{12}R_{CR}=^{12}R_{AOM} \quad (39)$$

$$^{13}F_{CH4.in}+^{13}R_{CR}=^{13}R_{AOM} \quad (40)$$

Since more than 90% of the in situ methane is lost during core recovery (Wallace et al., 2000), it is very unlikely to accurately determine methane flux (*i.e.,* $^{12}F_{CH4.in}$ and $^{13}F_{CH4.in}$). A slightly different in the degree of degassing would result in huge difference in flux estimation from headspace methane concentration gradient. Besides, the depth of gas hydrate first appearance is also adapted by some studies, such as Malinverno and Pohlman (2011), to be the constraint of methane flux since such depth should theoretically correspond to where dissolved methane concentration exceeds its solubility. However, as Torres et al. (2008) pointed out, the distribution of gas hydrate is also highly dependent on lithology. Such lithology-dependent control on gas hydrate distribution was observed in Ulleung Basin (UBGH2 scientists, 2010). Therefore, it may not be a proper approach. Alternatively, we constrain methane flux from its isotopic signature in order to solve another unknown in our equations. We consider this as a better approach since we focus here the isotopic signature of methane entering our model frame.

If we assume that methane concentration within the SMTZ ($^{13}C_{CH4\text{-}SMTZ}$ and $^{12}C_{CH4\text{-}SMTZ}$) is much lower than the methane at depth ($^{13}C_{CH4\text{-}bot}$ and $^{12}C_{CH4\text{-}bot}$) (Figure 1), we are able to relate the flux ratio of methane ($\frac{^{13}F_{CH_4.in}}{^{12}F_{CH_4.in}}$) to the concentration ratio of heavy to light methane carbon at the depth where $\delta^{13}C_{CH4}$ approaches a fixed value ($^{12/13}C_{CH4.bot}$ in Figure 1). This assumption allows us to combine Eqs. (39) and (40) in the following way:

$$\frac{^{13}F_{CH_4.in}}{^{12}F_{CH_4.in}}=\frac{\frac{^{13}C_{CH_4-bot}-^{13}C_{CH_4-SMTZ}}{L}}{\frac{^{12}C_{CH_4-bot}-^{12}C_{CH_4-SMTZ}}{L}}\cong\frac{^{13}C_{CH_4-bot}}{^{12}C_{CH_4-bot}}=r_{CH_4-bot}=\frac{^{13}R_{AOM}-^{13}R_{CR}}{^{12}R_{AOM}-^{12}R_{CR}} \quad (41)$$

where L is the depth between $C_{CH4\text{-}SMTZ}$ and $C_{CH4\text{-}bot}$ (Figure 1). From Eqs. (36), (37), (38), and (41), we can uniquely solve for the 4 unknowns ($R_{OM}$, $R_{AOM,}$ b, and $\alpha_{AOM}$). Except for Site UBGH2-10, the resulting value for $\alpha_{AOM}$ estimated with this approach (Figure 6) is higher than 1.03, which is out of the possible range suggested by Whiticar (1999). The unreasonably large $\alpha_{AOM}$ for most sites suggests, under the assumption in Case 3, more isotopically light DIC has to be produced in order to satisfy the mass balance. ME, which produces isotopically heavier DIC than the signature at SMTZ, may not be a suitable reaction at first glance. However, ME also produces isotopically light $CH_4$ which will be consumed and formed isotopically light DIC through AOM. Therefore, it is still logical to include this reaction.

*Case 4: Anaerobic oxidation of methane (AOM), particulate organic carbon sulfate reduction (POCSR), secondary methanogenesis by $CO_2$ reduction (CR) and methane generation from organic carbon (ME)*

We thus include ME in the box mode (Figure 5D). Since we must account for a fraction of organic matter being converted to methane (Eq. (7)), the fraction of organic matter that is consumed by sulfate reduction (*f* values in Eqs. (15) and (17)) is no longer 1 as in Case 1 to 3, but a number smaller than 1. The equation set for this case can be expressed as (Figure 5D):

$$F_{SO4.in}=R_{POCSR\text{-}S}+R_{AOM} \qquad (42)$$

$$^{12}F_{DIC.in}+{}^{12}R_{POCSR\text{-}C}+{}^{12}R_{AOM}+{}^{12}R_{ME\text{-}DIC}={}^{12}F_{DIC.out}+{}^{12}R_{CR}+{}^{12}R_{CP} \qquad (43)$$

$$^{13}F_{DIC.in}+{}^{13}R_{POCSR\text{-}C}+{}^{13}R_{AOM}+{}^{13}R_{ME\text{-}DIC}={}^{13}F_{DIC.out}+{}^{13}R_{CR}+{}^{13}R_{CP} \qquad (44)$$

$$\frac{^{13}F_{CH_4.in}}{^{12}F_{CH_4.in}} \cong \frac{^{13}C_{CH_4-bot}}{^{12}C_{CH_4-bot}} = \frac{^{13}R_{AOM}-{}^{13}R_{CR}-{}^{13}R_{ME-CH_4}}{^{12}R_{AOM}-{}^{12}R_{CR}-{}^{12}R_{ME-CH_4}} \qquad (45)$$

In addition to the 4 unknowns detailed in Case 3, we now have one more unknown, *f*. Therefore, we are not able to uniquely constrain the system with the available data. Nonetheless, we are able to evaluate the equation sets by varying *f* from 0 to 1 to determine the ranges of *f* for which $\alpha_{AOM}$ falls within a reasonable range, as illustrated by the data that lie within the dash lines in Figure 7A. We also calculated the possible

fraction of DIC from AOM that is recycled through CR (*i.e., b*), as shown in Figure 7B.

Our results suggest that:

1) In order to satisfy the isotopic mass balance (as inferred by agreement with $\alpha_{AOM}$ values from the literature), a significant fraction (>50% in 4 of the studied sites as the *f* is smaller than 0.5 in Figure 7A for these sites) of the organic matter is metabolized via methanogenesis (ME) rather than via sulfate reduction POCSR. Only at Site UBGH2-10 can we achieve isotopic compliance without ME; and

2) ME alone is not able to satisfy the isotopic mass balance, but in all cases a significant fraction (28 to 45%) of the DIC produced from AOM (*b* in Figure 7B) has to be recycled to methane by CR. This, however, is not what Chatterjee et al. (2011) concluded from their kinetic model that aims at achieving a mass balance with a full consideration of methane and DIC isotopic signatures. Our approach differs in that we specifically separate CR from ME in order to describe the cycling of carbon between methane and DIC pools, which influence the model results and hence leads to different interpretations. Although Chatterjee et al. (2011) also included isotopic signature of methane into their model, they did not track its change. Therefore, we are not able to verify the mass balance of their model based on the results presented.

# 6. Discussion

*Carbon cycling around the SMTZ in Ulleung Basin*

The relative contribution of the 5 individual reactions considered in ESMTZ to the overall DIC pool, has been estimated as the ratio of the reaction rates to the net DIC flux ($\Delta F_{DIC} = F_{DIC.in} - F_{DIC.out}$). The results at each of the study sites are depicted in Figure 8, and Table 5 summarizes the depth-integrated rates for each reaction. Except for Site UBGH2-10, the contribution of each reaction to DIC production is AOM>ME>POCSR. It is also apparent from these results that a fraction of the DIC produced by AOM is consumed by CR within the ESMTZ. To balance this DIC consumption, a similar rate of organic matter degradation becomes necessary, and as shown in Figure 8, the overall POCSR may be responsible for utilizing up to 30% of the total sulfate input from seafloor.

We conducted a series of correlation tests between the site-specific parameters (Table 1) and the model inputs (Table 3) and outputs (Table 5). Although correlation can not be used to infer consequential relationships, it is informative to identify the connected parameters. The results of this correlation test could be found in the supplementary material. It is interesting to note that the depth of the SMTZ depth is, as expected, inversely correlated with the sulfate flux ($r^2$=0.89) and with DIC flux above the SMTZ ($r^2$=0.92). It is, however, not distinctly correlated with any of the absolute reaction rates except for POCSR ($r^2$=0.61), which suggests a connection between the SMTZ depth and organic matter degradation rate rather than with the AOM rate. The average POC content is inversely correlated with the organic matter degradation rate ($r^2$=0.54) and with the methane carbon isotope at the SMTZ ($r^2$=0.51).

Bhatnagar et al. (2011) suggested that the depth of gas hydrate first occurrence is positively correlated with the SMTZ depth assuming fluid flow is the most dominant factor affecting both. However for the Ulleung Basin, neither the depths of BSR nor that of the gas hydrate first appearance shows any appreciable correlation with the SMTZ depth nor with the carbon or sulfate fluxes. Bhatnagar et al. (2011) shows that SMTZ depth and sulfate gradients may be used to infer the average gas hydrate saturation in the Cascadia margin system but only when all methane comes from a deep external reservoir (*e.g.*, gas hydrate) and AOM is the only sink of sulfate. Our box model results indicate that neither of these assumptions is valid in the Ulleung Basin, since POCSR consumes a significant fraction of sulfate and there is an important methane source that originates just below the SMTZ also contributes to the overall carbon cycling within the SMTZ. There is also no correlation between the AOM rate and gas hydrate abundance indicators (*i.e.*, depth of BSR and first gas hydrate appearance in Table 1), which suggests that the deep gas hydrate system (>70 mbsf) in these diffusion-dominated sites at Ulleung Basin is too remote to effectively influence the shallow (< 30 mbsf) carbon cycles around the SMTZ. Thus, in the sites discussed here, the AOM rates cannot be used to quantify methane contributions from gas hydrate reservoirs that lay tens to hundreds of meters below the SMTZ. Nonetheless, we speculate that the advective systems that characterize acoustic chimney locations in the Ulleung Basin (Torres et al., 2011; Kim et al., 2011, 2012) will indeed have a profound influence on the carbon cycling around the SMTZ.

*Evidence for coupling AOM and CR in natural and laboratory studies*

Carbon cycling through an AOM-CR coupled pathway at the SMTZ, was originally proposed by Borowski et al. (1997), based on observations of anomalously light carbon isotopic values of DIC and methane around the SMTZ in samples collected by Ocean Drilling Program at the Blake Ridge (Claypool and Threlkeld, 1983; Galimov and Kvenvolden, 1983). Since then, an anomalously light carbon isotopic signature of microbial biomass (House et al., 2009) and lipid biomarkers (Orcutt et al., 2005; Alperin and Hoehler, 2009) near the SMTZ, have been used as an important AOM-CR coupling indicator, because the measured fractionations cannot be explained solely from organic carbon degradation, and require fractionation by methanogens (Alperin and Hoehler, 2009).

Direct evidence for the existence of this AOM-CR coupling was presented by Zehnder and Brock (1979, 1980), who quantified both reactions simultaneously in culture experiments. Radiotracer experiments have also shown that the CR rate is not only of comparable magnitude to that of AOM, in some cases, these rates are shown to be proportional to each other (Pimenov et al., 1997; Orcutt et al., 2005; Seifert et al., 2006; Knab et al., 2009) and maybe a function of the methane and sulfate availability (Orcutt et al., 2008).

Hoehler et al. (1994) postulated that the methanogenic archaea, which mediate AOM, may be able to switch their metabolism between methanogenesis and methanotrophy depending on the fluid composition, and thus may thermodynamically favor one pathway over the other. In addition, metagenomic studies of communities collected from the SMTZ indicate that methanotrophic archaea possess most of the genes that are typically required for methanogenesis thus supporting the hypothesis that these microbes are capable of carrying out "reverse methanogenesis" (Hallam et al. 2004). Whether methanogenic archaea can indeed switch their metabolic pathway is still debated. However, rDNA and rRNA maxima at and immediately below the SMTZ, were used by Lloyd et al. (2011) to reinforce the idea that ANME-1 may indeed be capable of consuming and producing methane, and that the dominant metabolic pathway does depend on the attendant geochemical environment.

Of course, for CR to precede an additional source of $H_2$ is needed. We do not know that the $H_2$ source has been established; however, the aforementioned studies all show the coupling between AOM and CR to be highly prevalent. The actual metabolic pathways and the organisms involved are still being debated by the geomicrobiology community; however, it is becoming more and more apparent that the AOM and CR reaction rates are interdependent and are controlled by the methane and sulfate availability. These observations and the results of our box model indicate that it is necessary to take this important carbon cycling pathway into consideration in future studies aimed at unraveling processes at, and immediately below, the SMTZ.

*Future improvements*

We were not able to uniquely solve all 5 reactions involved in the cycling of carbon (Case 4), due to lack of additional data. Quantification of the 5 unknowns ($R_{OM}$, $R_{AOM}$, $b$, $\alpha_{AOM}$, and $f$) from field or experimental studies, would allow us to fully constrain the system. Alternatively, we can also use robust data on the in situ methane concentrations, which would allow us to confidently estimate the methane fluxes from beneath the ESMTZ ($C_{CH4\text{-}bot}$ or $F_{CH4.in}$ in Figure 4A). This in situ methane concentration may be obtained by sampling the sediments with a pressure core sampler (PCS) that maintains the in-situ conditions. Results from Case 3 and 4 also emphasize the need of incorporating the methane isotopic composition to fully constrain the carbon metabolic pathways in the SMTZ. These data have not been included in previous studies (Snyder et al., 2007) or its significance was not fully appreciated (Chatterjee et al., 2011; Malinverno and Pohlman, 2011).

# 7. Conclusion

Sulfate gradients have been used as an important proxy to quantify the methane supply from deep reservoirs such as gas hydrate, which is critical to fully constrain carbon cycling in marine sediments. However, the commonly used assumption that sulfate gradients are fully coupled to the anaerobic oxidation of methane (AOM) is complicated by the sulfate consumption from organic matter degradation (POCSR),

and carbon cycling between pools of methane and dissolved inorganic carbon (DIC) via and $CO_2$ reduction (CR).

We developed a box model, which incorporates stoichiometry, flux, and isotopic mass balances, to constrain the relative proportion of the five reactions involved the cycling of carbon within the SMTZ. We show that in the Ulleung Basin, more than half of the DIC input to the SMTZ is directly related to organic matter degradation (either via sulfate reduction, POCSR, or methanogenesis (ME), while AOM is responsible for the rest of DIC flux. The fraction of DIC that is reduced to methane via a secondary methanogenesis (*i.e.,* CR) within the SMTZ ranges from 25 to 35%, and the methane produced by this reaction will further feed AOM.

By including isotopic considerations in our model, the quantification of organic matter degradation and of the cycling of carbon between the DIC and methane pools (through AOM and CR) revealed that the rates of AOM and sulfate reduction are not necessary equal to each other, as would be suggested by mass fluxes alone. Instead, the fraction of sulfate consumed by AOM ranges from 70 to 90%. Therefore, whereas first order relative estimates of methane fluxes can be made based solely on sulfate data, such methane flux estimates may have errors that range from 10 to 30%.

Isotopic data was also the key in documenting that AOM is not supported in its entirety by a methane flux into the SMTZ from deep sources, rather a significant contribution of this methane originates immediately below the SMTZ. Thus, at least in the Ulleung Basin, the SMTZ depth by itself cannot be used as a quantitative indicator of methane supplied from gas hydrate reservoirs, as it has been postulated for other gas hydrate bearing locations.

# 8. Acknowledgements

The authors would like to thank the co-chief scientists (Byong-Jae Ryu, Timothy S. Collett, and Michael Riedel), the captain, crew members, and shipboard scientific party of the D/V Fugro Synergy for the excellent support they provided during the 2010 UBGH2 Expedition. This project was made possible with the funding support from Korea Institute of Geosciences and Mineral Resources (KIGAM) (GP2012-026) and US Department of Energy, National Energy Technology Lab under RES

697 contract (DE-FE0004000). The authors would also like to thank Dr. Reimers and three anonymous
698 reviewers for valuable comments to the manuscript.

# Reference


Alperin MJ & Hoehler TM (2009) Anaerobic Methane Oxidation by Archaea/sulfate-Reducing Bacteria Aggregate: 2. Isotopic Constraints. American Journal of Science 309: 958-984

Bahk J-J, Kim J-H, Kong G-S, Park Y, Lee H, Park Y & Park KP (2009) Occurrence of near-seafloor gas hydrates and associated cold vents in the Ulleung Basin, East Sea. Geosciences Journal 13: 371-385

Bhatnagar G, Chatterjee S, Chapman WG, Dugan B, Dickens GR & Hirasaki GJ (2011) Analytical theory relating the depth of the sulfate-methane transition to gas hydrate distribution and saturation. Geochemistry Geophysics Geosystems 12: Q03003, doi:10.1029/2010GC003397.

Borowski WS, Paull CK & Ussler W (1996) Marine pore-water sulfate profiles indicate in situ methane flux from underlying gas hydrate. Geology 24: 655-658

Borowski WS, Paull CK & Ussler W (1997) Carbon cycling within the upper methanogenic zone of continental rise sediments: An example from the methane-rich sediments overlying the Blake Ridge gas hydrate deposits. Marine Chemistry 57: 299-311

Borowski WS, Paull CK & Ussler W (1999) Global and local variations of interstitial sulfate gradients in deep-water, continental margin sediments: Sensitivity to underlying methane and gas hydrates. Marine Geology 159: 131-154

Boudreau BP (1997) Diagenetic models and their implementation: modeling transport and reactions in aquatic sediments. Springer, 414pp.

Chatterjee S, Dickens GR, Bhatnagar G, Chapman WG, Dugan B, Snyder GT & Hirasaki GJ (2011) Pore water sulfate, alkalinity, and carbon isotope profiles in shallow sediment above marine gas hydrate systems: A numerical modeling perspective. Journal of Geophysical Research-Solid Earth 116, B09103, doi:10.1029/2011JB008290.

Chuang PC, Yang TF, Hong WL, Lin S, Sun CH, Lin ATS, Chen JC, Wang Y & Chung SH (2010) Estimation of methane flux offshore SW Taiwan and the influence of tectonics on gas hydrate accumulation. Geofluids 10: 497-510

Chuang PC, Yang TF, Lin S, Lee HF, Lan TFF, Hong WL, Liu CS, Chen JC & Wang Y (2006) Extremely high methane concentration in bottom water and cored

731 sediments from offshore southwestern Taiwan. Terrestrial Atmospheric and
732 Oceanic Sciences 17: 903-920
733 Chun J-H, Ryu B-J, Son B-K, Kim J-H, Lee JY, Bahk J-J, Kim H-J, Woo KS &
734 Nehza O (2011) Sediment mounds and other sedimentary features related to
735 hydrate occurrences in a columnar seismic blanking zone of the Ulleung Basin,
736 East Sea, Korea. Marine and Petroleum Geology 28: 1787-1800
737 Claypool GE, Milkov AV, Lee YJ, Torres ME, Borowski WS & Tomaru H (2006)
738 Microbial methane generation and gas transport in shallow sediments of an
739 accretionary complex, southern Hydrate Ridge (ODP Leg 204), offshore
740 Oregon, USA. In: Bohrmann G, Tréhu AM, Torres ME & Colwell FS (Eds)
741 Proceeding Ocean Drilling Program Scientific Results.
742 Claypool GE & Threlkeld CN (1983) Anoxic Diagenesis and Methane Generation in
743 Sediments of the Blake Outer Ridge, Deep-Sea Drilling Project Site-533,
744 Leg-76. Initial Reports of the Deep Sea Drilling Project 76: 391-402
745 Colwell FS, Boyd S, Delwiche ME, Reed DW, Phelps TJ & Newby DT (2008)
746 Estimates of biogenic methane production rates in deep marine sediments at
747 Hydrate Ridge, Cascadia margin. Applied and Environmental Microbiology 74:
748 3444-3452
749 Dickens GR (2001) Sulfate profiles and barium fronts in sediment on the Blake
750 Ridge: Present and past methane fluxes through a large gas hydrate reservoir.
751 Geochim. Cosmochim. Acta 65: 529-543
752 Fossing H, Ferdelman TG & Berg P (2000) Sulfate reduction and methane oxidation
753 in continental margin sediments influenced by irrigation (South-East Atlantic off
754 Namibia). Geochim. Cosmochim. Acta 64: 897-910
755 Galimov EM & Kvenvolden KA (1983) Concentrations and Carbon Isotopic
756 Compositions of $CH_4$ and $CO_2$ in Gas from Sediments of the Blake Outer Ridge,
757 Deep-Sea Drilling Project Leg-76. Initial Reports of the Deep Sea Drilling
758 Project 76: 403-407
759 Hallam SJ, Putnam N, Preston CM, Detter JC, Rokhsar D, Richardson PM & DeLong
760 EF (2004) Reverse methanogenesis: Testing the hypothesis with environmental
761 genomics. Science 305: 1457-1462
762 Hoehler TM, Alperin MJ, Albert DB & Martens CS (1994) Field and Laboratory
763 Studies of Methane Oxidation in an Anoxic Marine Sediment - Evidence for a

764 Methanogen-Sulfate Reducer Consortium. Global Biogeochemical Cycles 8:
765 451-463
766 House CH, Orphan VJ, Turk KA, Thomas B, Pernthaler A, Vrentas JM & Joye SB
767 (2009) Extensive carbon isotopic heterogeneity among methane seep
768 microbiota. Environmental Microbiology 11: 2207-2215
769 Jahne B, Heinz G & Dietrich W (1987) Measurement of the Diffusion-coefficients of
770 Sparingly Soluble Gases in Water. Journal of Geophysical Research-Oceans 92:
771 10767-10776
772 Jørgensen BB, Weber A & Zopfi J (2001) Sulfate reduction and anaerobic methane
773 oxidation in Black Sea sediments. Deep-Sea Research Part I-Oceanographic
774 Research Papers 48: 2097-2120
775 Kim J-H, Park M-H, Tsunogai U, Cheong T-J, Ryu B-J, Lee Y-J, Han H-C, Oh J-H &
776 Chang H-W (2007) Geochemical characterization of the organic matter, pore
777 water constituents and shallow methane gas in the eastern part of the Ulleung
778 Basin, East Sea (Japan Sea). Island Arc 16: 93-104
779 Kim JH, Park MH, Chun JH & Lee JY (2011) Molecular and isotopic signatures in
780 sediments and gas hydrate of the central/southwestern Ulleung Basin: high
781 alkalinity escape fuelled by biogenically sourced methane. Geo-Marine Letters
782 31: 37-49
783 Kim JH, Torres ME, Choi J, Bahk JJ, Park MH & Hong WL (2012) Inferences on gas
784 transport based on molecular and isotopic signatures of gases at acoustic
785 chimneys and background sites in the Ulleung Basin. Organic Geochemistry 43:
786 26-38
787 Knab NJ, Cragg BA, Hornibrook ERC, Holmkvist L, Pancost RD, Borowski C,
788 Parkes RJ & Jorgensen BB (2009) Regulation of anaerobic methane oxidation in
789 sediments of the Black Sea. Biogeosciences 6: 1505-1518
790 Lin S, Hsieh WC, Lim YC, Yang TF, Liu CS & Wang Y (2006) Methane migration
791 and its influence on sulfate reduction in the Good Weather Ridge region, South
792 China Sea continental margin sediments. Terrestrial Atmospheric and Oceanic
793 Sciences 17: 883-902
794 Lloyd KG, Alperin MJ & Teske A (2011) Environmental evidence for net methane
795 production and oxidation in putative ANaerobic MEthanotrophic (ANME)
796 archaea. Environmental Microbiology 13: 2548-2564

797 Malinverno A, Kastner M, Torres ME & Wortmann UG (2008) Gas hydrate
798 occurrence from pore water chlorinity and downhole logs in a transect across the
799 northern Cascadia margin (Integrated Ocean Drilling Program Expedition 311).
800 Journal of Geophysical Research-Solid Earth 113, B08103, doi:
801 10.1029/2008jb005702
802 Malinverno A & Pohlman JW (2011) Modeling sulfate reduction in methane
803 hydrate-bearing continental margin sediments: Does a sulfate-methane transition
804 require anaerobic oxidation of methane? Geochemistry Geophysics Geosystems
805 12, Q07006, doi: 10.1029/2011gc003501
806 Manheim FT & Sayles FL (1974) Composition and origin of interstitial waters of
807 marine sedimnets, based on Deep Sea Drill Cores. In: Goldberg ED (Ed) The
808 sea pp 527-568). John Wiley & Sons, New York
809 Niewohner C, Hensen C, Kasten S, Zabel M & Schulz HD (1998) Deep sulfate
810 reduction completely mediated by anaerobic methane oxidation in sediments of
811 the upwelling area off Namibia. Geochim. Cosmochim. Acta 62: 455-464
812 Oleary MH (1984) Measurement of the Isotope Fractionation Associated with
813 Diffusion of Carbon-dioxide in Aqueous Solution. Journal of Physical
814 Chemistry 88: 823-825
815 Orcutt B, Boetius A, Elvert M, Samarkin V & Joye SB (2005) Molecular
816 biogeochemistry of sulfate reduction, methanogenesis and the anaerobic
817 oxidation of methane at Gulf of Mexico cold seeps. Geochim. Cosmochim. Acta
818 69: 4267-4281
819 Orcutt B, Samarkin V, Boetius A & Joye S (2008) On the relationship between
820 methane production and oxidation by anaerobic methanotrophic communities
821 from cold seeps of the Gulf of Mexico. Environmental Microbiology 10:
822 1108-1117
823 Oremland RS, Marsh LM & Polcin S (1982) Methane Production and Simultaneous
824 Sulfate Reduction in Anoxic, Salt-marsh Sediments. Nature 296: 143-145
825 Pimenov NV, Rusanov I, Poglazova MN, Mityushina LL, Sorokin DY, Khmelenina
826 VN & Trotsenko YA (1997) Bacterial mats on coral-like structures at methane
827 seeps in the Black Sea. Microbiology 66: 354-360
828 Rees CE (1973) Steady-State Model for Sulfur Isotope Fractionation in Bacterial
829 Reduction Processes. Geochim. Cosmochim. Acta 37: 1141-1162

Riedel M, Novosel I, Spence GD, Hyndman RD, Chapman RN, Solem RC & Lewis T (2006) Geophysical and geochemical signatures associated with gas hydrate-related venting in the northern Cascadia margin. Geological Society of America Bulletin 118: 23-38

Scientists U (2010) Ulleung Basin Gas Hydrate Drilling Expedition 2. Preliminary Report. Daejeon, Republic of Korea, KIGAM

Seifert R, Nauhaus K, Blumenberg M, Krueger M & Michaelis W (2006) Methane dynamics in a microbial community of the Black Sea traced by stable carbon isotopes in vitro. Organic Geochemistry 37: 1411-1419

Snyder GT, Hiruta A, Matsurnoto R, Dickens GR, Tomaru H, Takeuchi R, Komatsubara J, Ishida Y & Yu H (2007) Pore water profiles and authigenic mineralization in shallow marine sediments above the methane-charged system on Umitaka Spur, Japan Sea. Deep-Sea Research Part Ii-Topical Studies in Oceanography 54: 1216-1239

Torres ME, Kim J-H, Choi J-Y, Ryu B-J, Bahk J-J, Riedel M, Collett T, Hong W-L & Kastner M (2011) Occurrence of High Salinity Fluids Associated with Massive Near-seafloor Gas Hydrate Deposits. 7th International Conference on Gas Hydrates. Edinburgh, Scotland, United Kingdom

Torres ME, Mix AC & Rugh WD (2005) Precise delta C-13 analysis of dissolved inorganic carbon in natural waters using automated headspace sampling and continuous-flow mass spectrometry. Limnology and Oceanography-Methods 3: 349-360

Torres ME, Trehu AM, Cespedes N, Kastner M, Wortmann UG, Kim JH, Long P, Malinverno A, Pohlman JW, Riedel M & Collett T (2008) Methane hydrate formation in turbidite sediments of northern Cascadia, IODP Expedition 311. Earth Planet. Sci. Lett. 271: 170-180

UBGH2 Scientists (2010) Ulleung Basin Gas Hydrate Drilling Expedition 2. Preliminary Report. Daejeon, Republic of Korea, KIGAM

Wallace PJ, Dickens GR, Paull CK & Ussler W (2000) Effects of Core Retrieval and Degassing on the Carbon Isotope Composition of Methane in Gas Hydrate- and Free Gas- Bearing Sediments from Blake Ridge. In: Paul CK, Matumoto R, Wallace PJ & Oillon WP (Eds) Proceedings of the Ocean Drilling Program, Scientific Results.

Wehrmann LM, Risgaard-Petersen N, Schrum HN, Walsh EA, Huh Y, Ikehara M, Pierre C, D'Hondt S, Ferdelman TG, Ravelo AC, Takahashi K, Zarikian CA & Integrated Ocean Drilling P (2011) Coupled organic and inorganic carbon cycling in the deep subseafloor sediment of the northeastern Bering Sea Slope (IODP Exp. 323). Chem. Geol. 284: 251-261

Whiticar MJ (1999) Carbon and hydrogen isotope systematics of bacterial formation and oxidation of methane. Chem. Geol. 161: 291-314

Yang T, Jiang SY, Yang JH, Lu G, Wu NY, Liu J & Chen DH (2008) Dissolved inorganic carbon (DIC) and its carbon isotopic composition in sediment pore waters from the Shenhu area, northern South China Sea. Journal of Oceanography 64: 303-310

Zeebe RE & Wolf-Gladrow D (2001) CO2 in Seawater Equilibrium, Kinetics, Isotopes. Elsevier Science,

Zehnder AJB & Brock TD (1979) Methane Formation and Methane Oxidation by Methanogenic Bacteria. Journal of Bacteriology 137: 420-432

Zehnder AJB & Brock TD (1980) Anaerobic Methane Oxidation- Occurrence and Ecology. Applied and Environmental Microbiology 39: 194-204

**Figure Captions**

Figure 1: The definitions of SMTZ and ESMTZ considered in our model. ESMTZ stands for Expanded Sulfate Methane Transition Zone that includes the shollow methanogenic zone right below the SMTZ.

Figure 2: Map of the UBGH2 drill sites in the Ulleung Basin. (A) Regional map of the basin. (B) The five sites investigated in this study.

Figure 3: Porosity profiles of the study sites. Black dots are onboard measurements while black lines are fitted profile using the parameters listed in Table 2.

Figure 4: Pore water profiles of data available for the box model. Red arrows illustrate the flux terms used in our box model. $r_{CH4.SMTZ}$, $r_{DIC.SMTZ}$ are $^{12}C/^{13}C$ of DIC or $CH_4$ that are calculated from isotopic values.

Figure 5: Framework of our box model. (A) Illustration of box model for Case 1, which only considers AOM and CP with in the SMTZ. (B) POCSR is added into the box in addition to the reactions considered in Case 1. (C) CR is included in the box model in addition to the reactions considered in Case 2. (D) ME is included in Case 4 which requires expanding the SMTZ (*i.e.,* ESMTZ) in this case.

Figure 6: The isotopic fractionation factors for AOM ($\alpha_{AOM}$) calculated from our box model based on the 4 different settings. The green area indicates range of fractionation factors from the literature (1.004-1.03; Whitcar, 1999). In Case 1 and 2, the fractionation factors are notably lower than expected. For Case 3, only the value for the site UBGH2-10 falls in the reasonable range; the rest are distinctly higher than expected range of value. The fractionation factors for sites UBGH2-1_1 and UBGH2-5 are much larger than 2; thus, they are not plotted in the figure. All the fractionation factors calculated from all sites in Case 4 agree well with the expected range indicating that isotopic mass balance is satisfied in this setting.

914 Figure 7: (A) Relationship between fraction of organic matter that is consumed by
915 sulfate reduction (*f*) and isotopic fractionation of AOM ($\alpha_{AOM}$). The horizontal dash
916 line marks the range of $\alpha_{AOM}$ from literature (Whiticar, 1999). The vertical dash line
917 marks the result of Case 3 which assumes all organic matter is consumed through
918 POCSR. (B) Relationship between the fraction of organic matter that is consumed by
919 sulfate reduction (*f*) and the fraction of DIC that is recycled by AOM (*b*) at each of the
920 five sites. Only the *f* values that result in the literature $\alpha_{AOM}$ values in (A) are plotted
921 here.
922
923 Figure 8: The relative contribution of each reaction. In the left panel, the contribution
924 from the five reactions studied are normalized with different DIC fluxes
925 ($\Delta F_{DIC}=F_{DIC.in}-F_{DIC.out}$). In the right panel, the fraction of sulfate that is consumed
926 through AOM is plotted. The bars at the top of each column represent the range of
927 contributions.
928
929

Figure1
Click here to download high resolution image

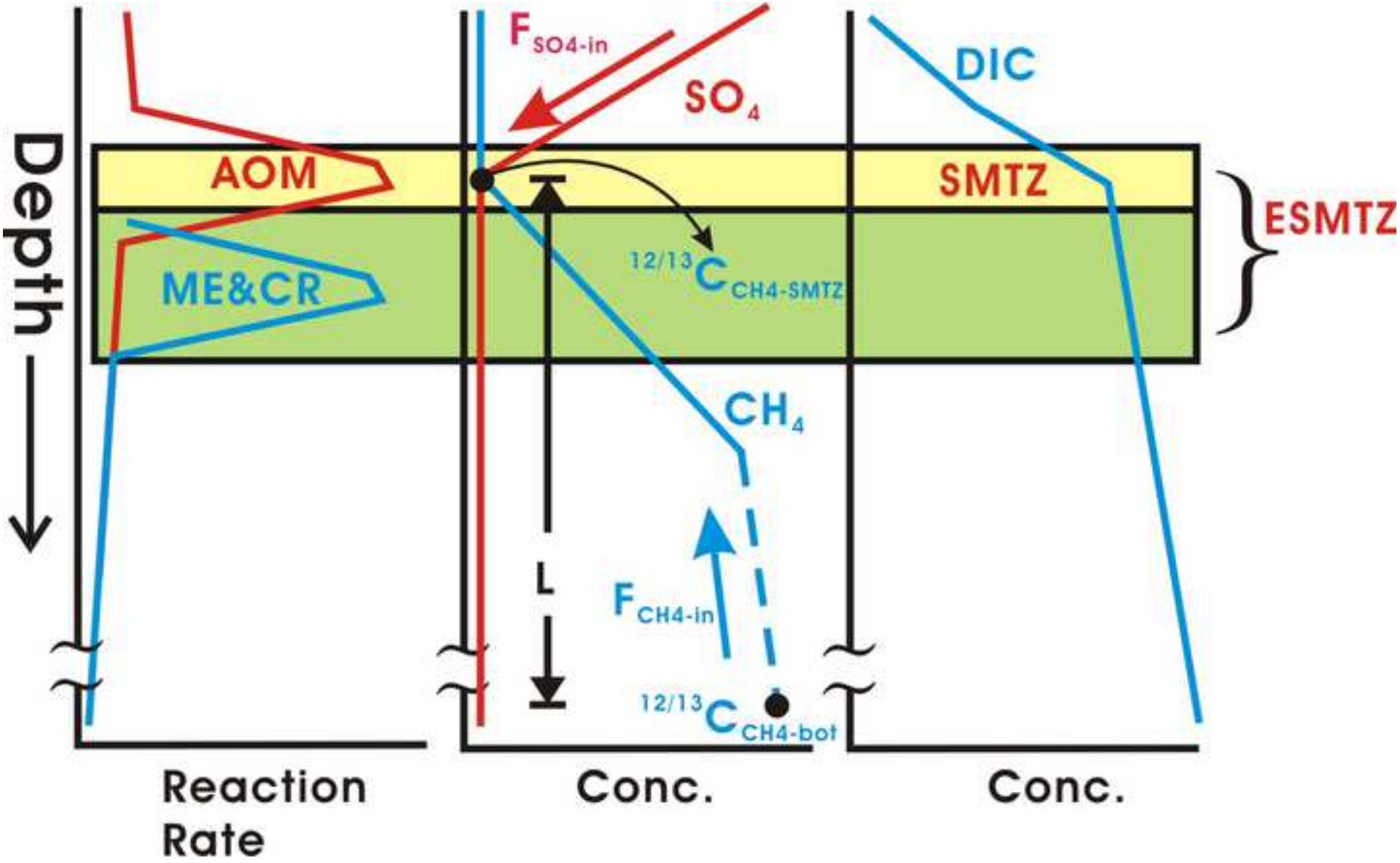

Figure2
Click here to download high resolution image

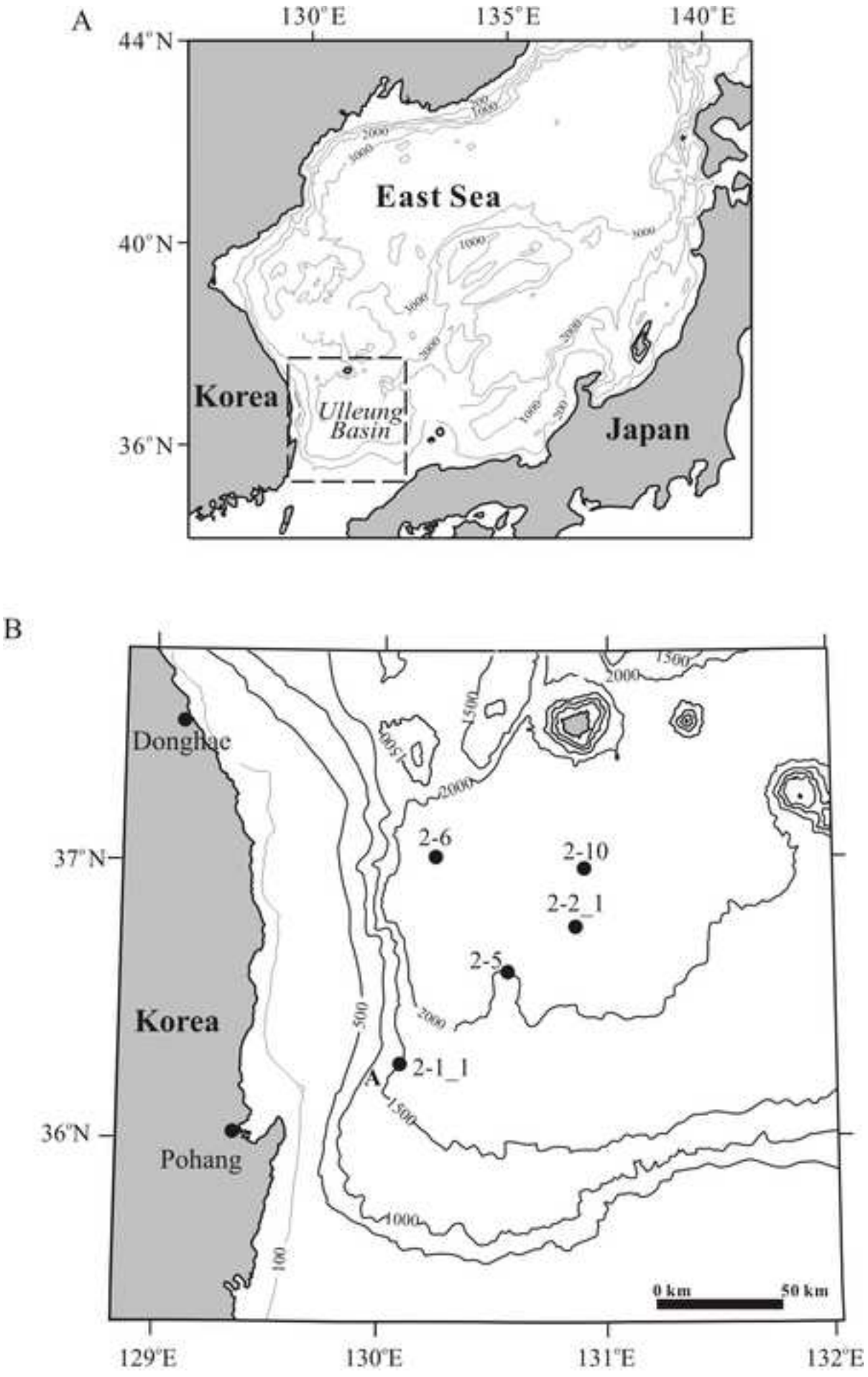

Figure3
Click here to download high resolution image

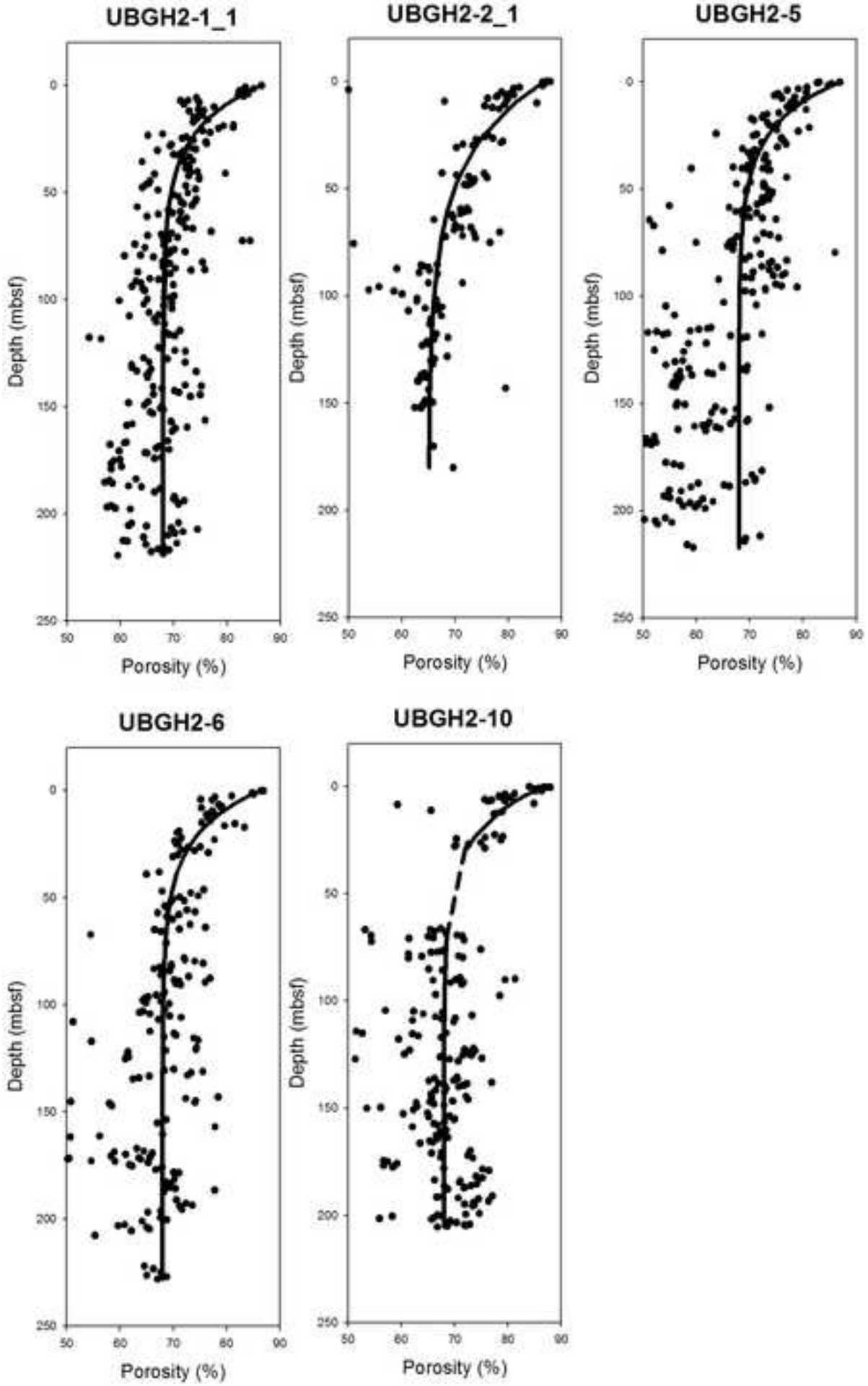

Figure4
Click here to download high resolution image

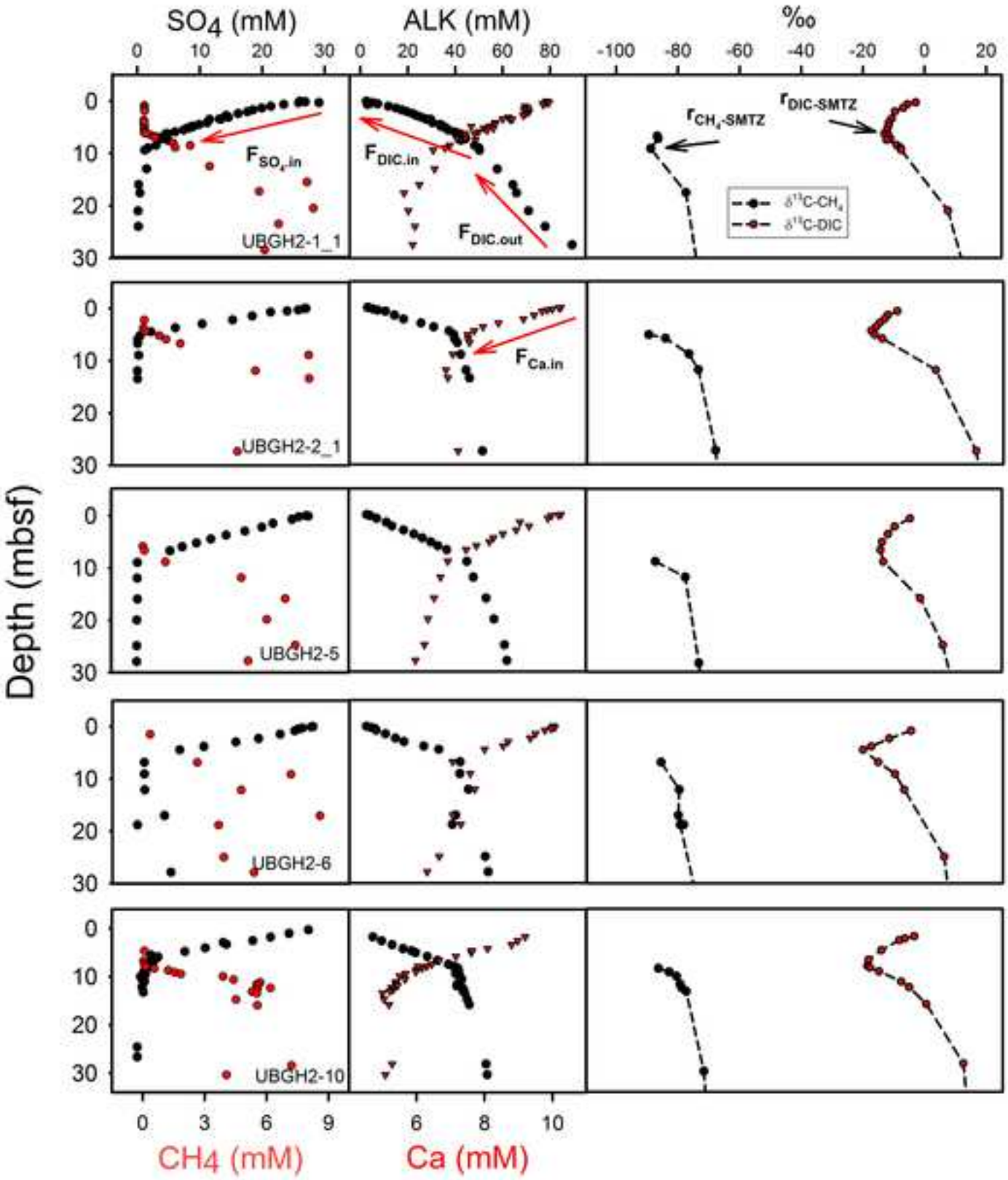

Figure5
Click here to download high resolution image

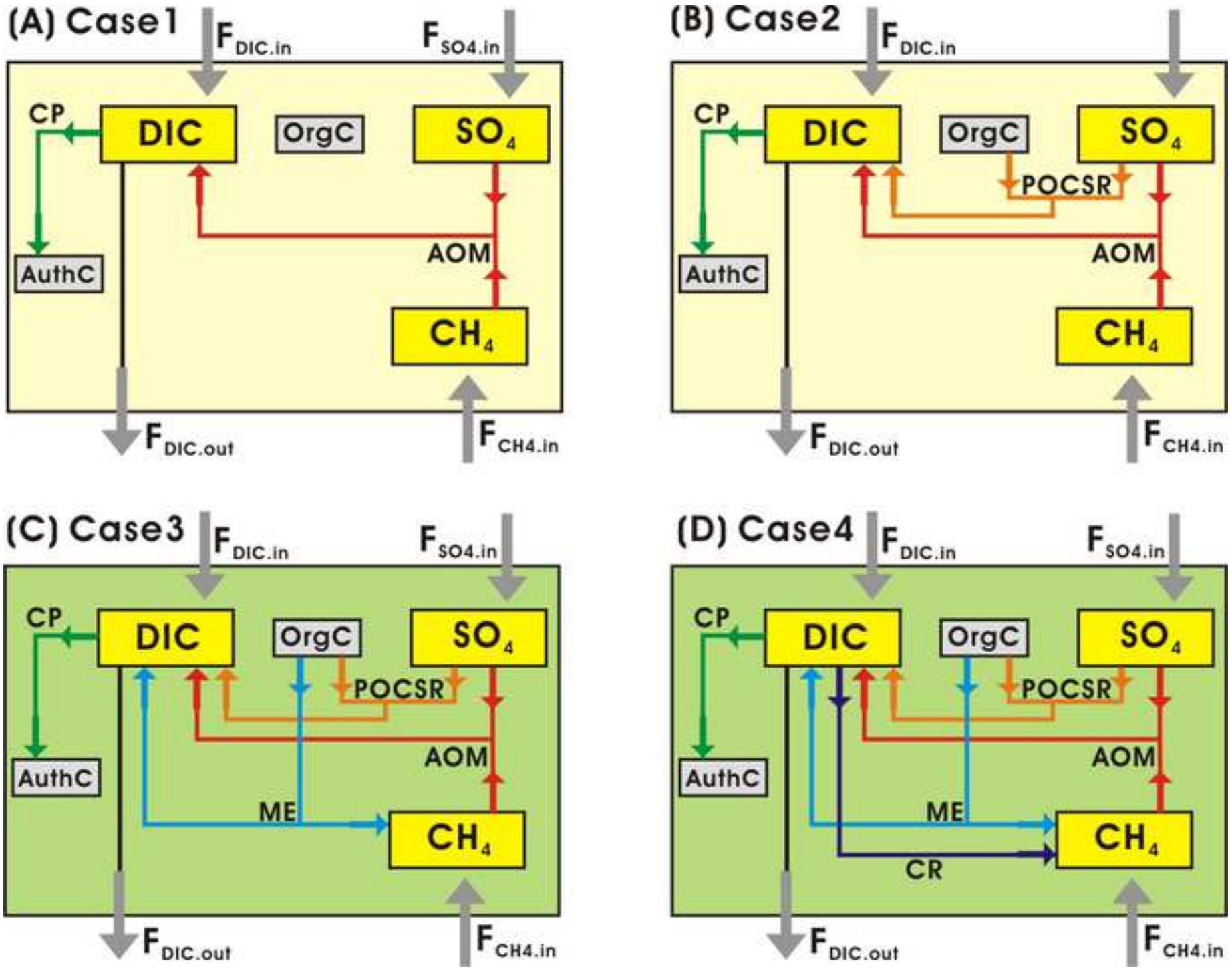

Figure6
Click here to download high resolution image

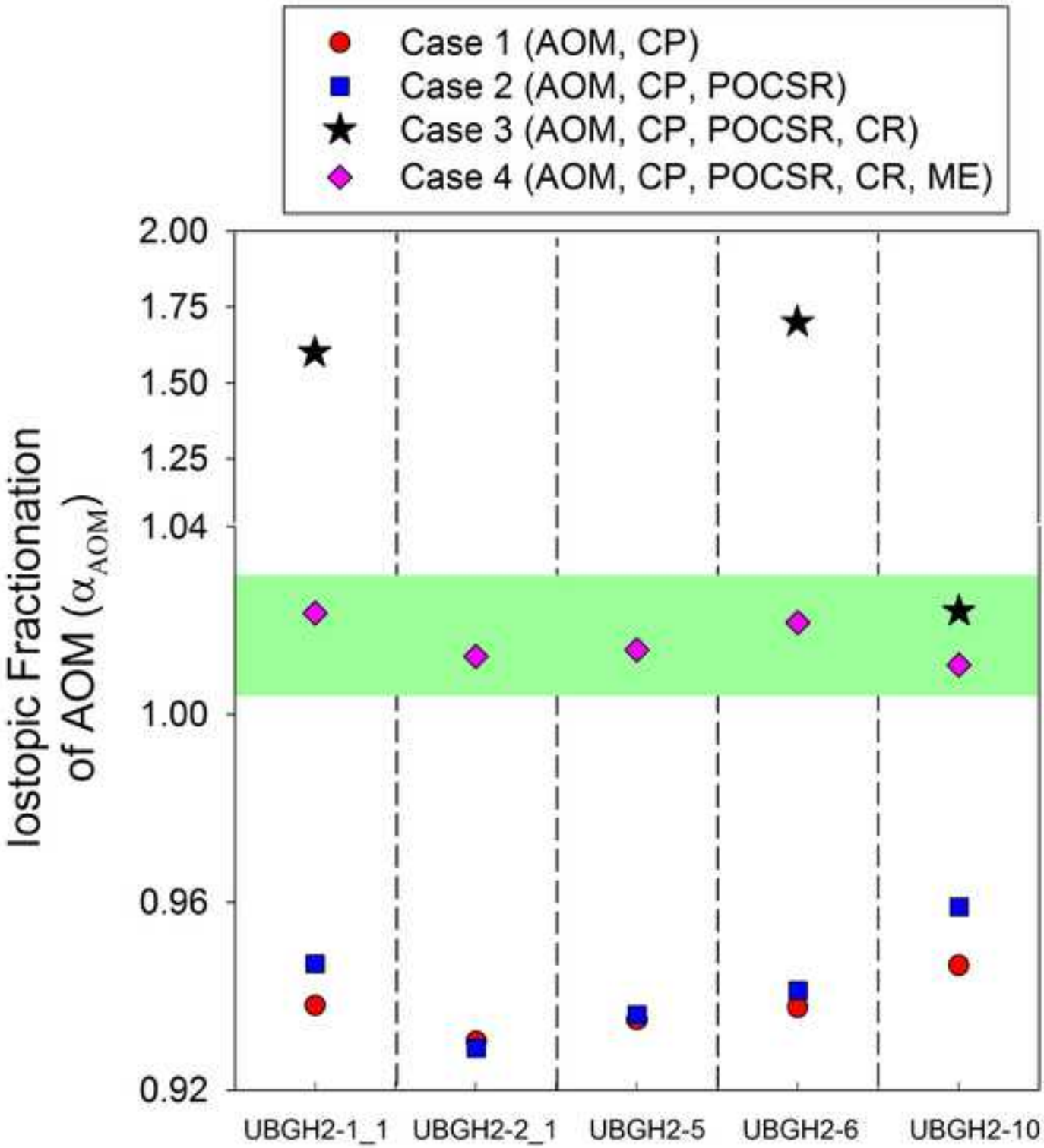

Figure7
Click here to download high resolution image

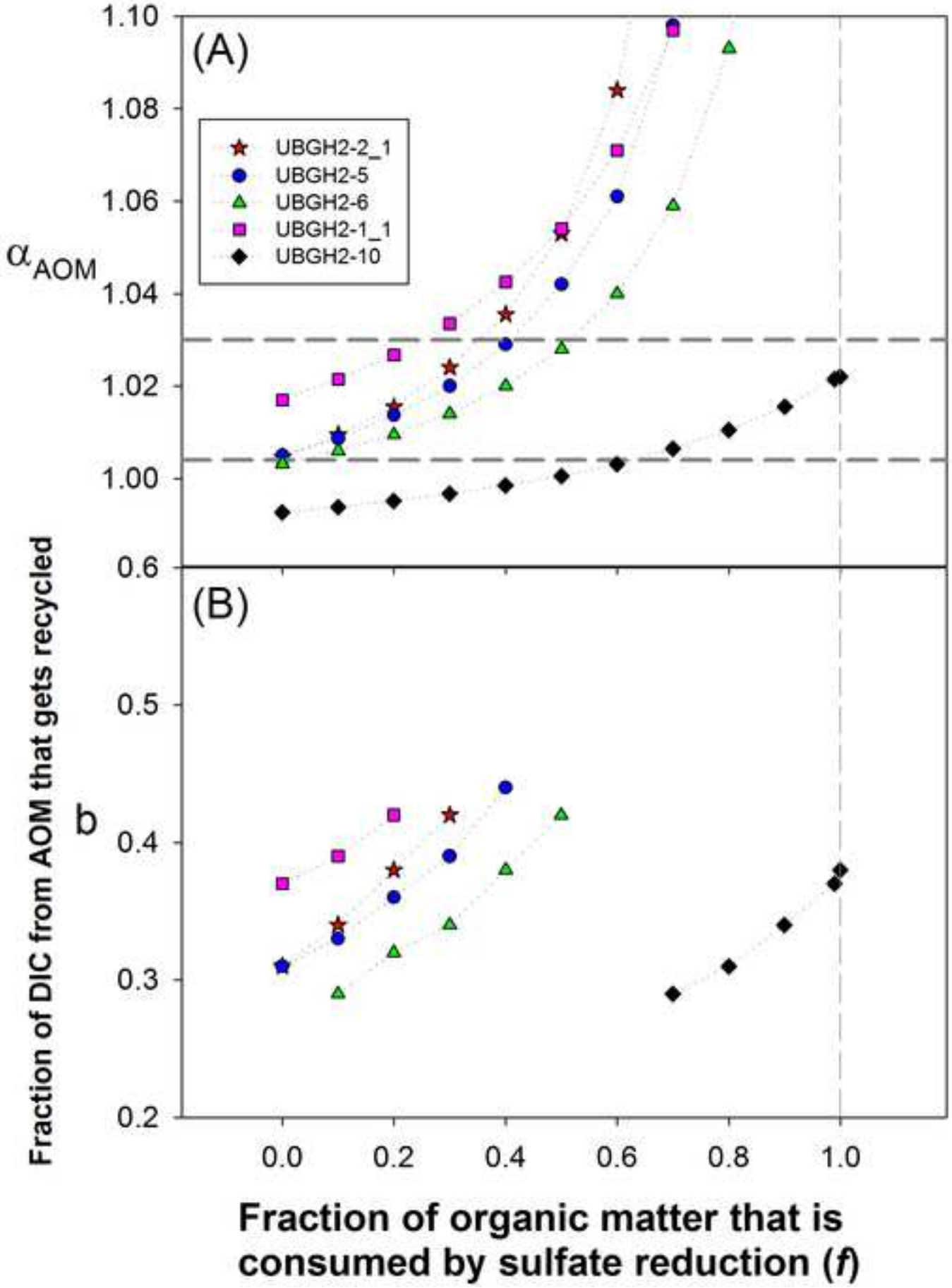

Figure8
Click here to download high resolution image

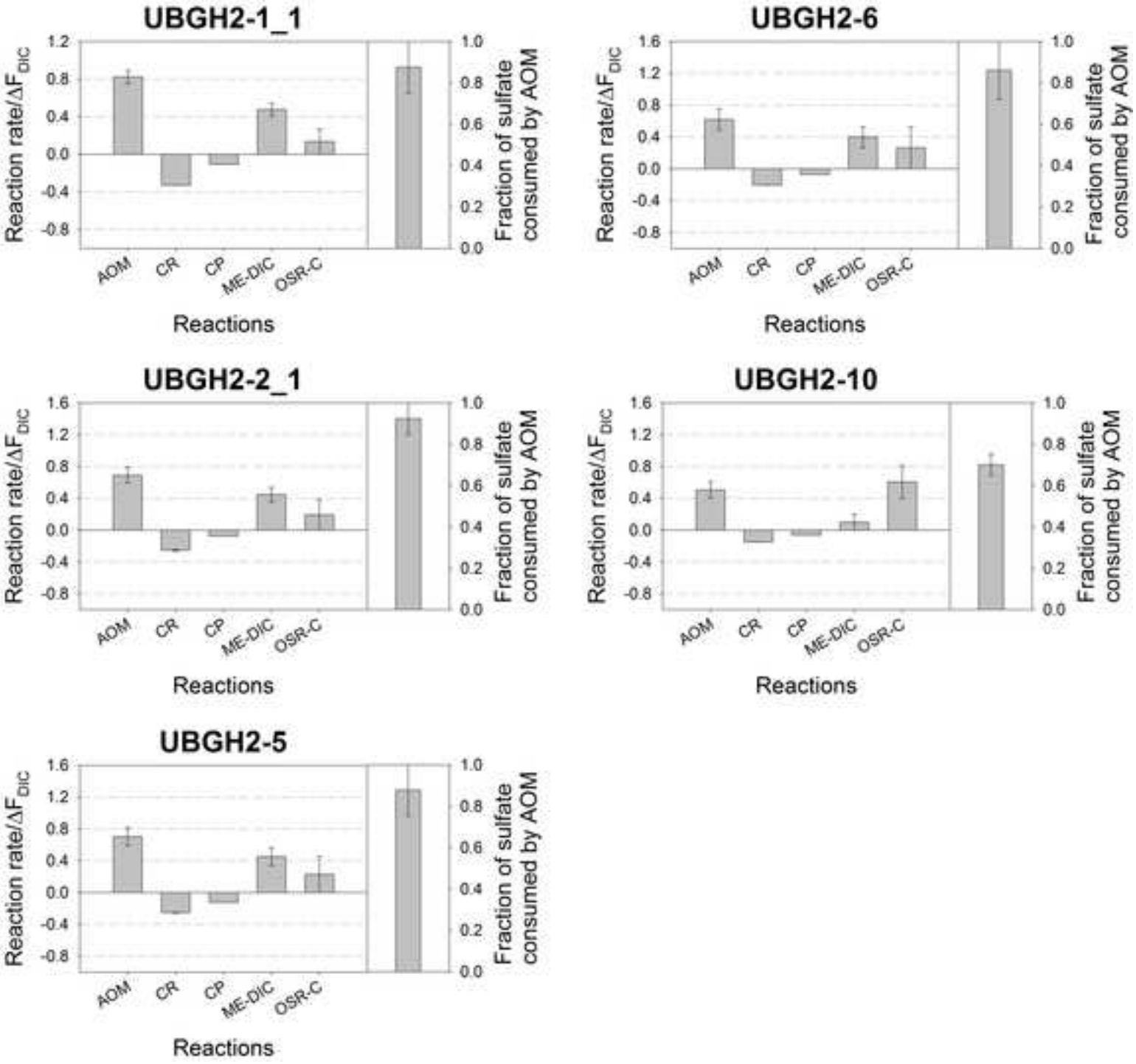

Table1
Click here to download Table: table1.pdf

Table 1 Depth of the BSR, first appearance of gas hydrate and the SMTZ, as well as organic carbon content of the study sites

| Site | BSR (mbsf) | First GH appearance depth (mbsf) | Depth of the SMTZ (mbsf) | POC (wt%) | | |
|---|---|---|---|---|---|---|
| | | | | Min. | Average | Max. |
| **UBGH2-1_1** | 165 | 93 | 7.7 | 0.62 | 1.93 | 4.03 |
| **UBGH2-2_1** | 176 | 71 | 7.0 | 0.31 | 1.59 | 3.66 |
| **UBGH2-5** | 189.5 | 153 | 8.0 | 0.16 | 1.30 | 3.91 |
| **UBGH2-6** | 167 | 113 | 6.6 | 0.09 | 1.23 | 4.15 |
| **UBGH2-10** | 171 | 77 | 6.2 | 0.21 | 1.40 | 3.44 |

Table2
Click here to download Table: table2.pdf

Table 2 Parameters used to fit the porosity profiles shown in Figure 2

| Site | Initial porosity at water-sediment interface $\phi_0$ (%) | Final porosity at depth $\phi_f$ (%) | empirical constant for data fitting $\gamma$ |
|---|---|---|---|
| **UBGH2-1_1** | 86.50 | 68.00 | -0.05 |
| **UBGH2-2_1** | 87.00 | 65.00 | -0.03 |
| **UBGH2-5** | 86.97 | 68.00 | -0.05 |
| **UBGH2-6** | 86.48 | 68.00 | -0.05 |
| **UBGH2-10** | 86.74 | 68.00 | -0.05 |

Table3
Click here to download Table: table3.pdf

Table 3 Fluxes (positive for upward flow) of various solutes across the SMTZ calculated from pore water profiles, DIC and $CH_4$ carbon isotopes at the SMTZ and at the core bottom for each of the 5 sites investigated in the Ulleung Basin. See text for the detailed definition of each term.

| Site | $^{12}F_{DIC.in}$ (μmol/cm$^2$/yr) | $^{12}F_{DIC.out}$ (μmol/cm$^2$/yr) | $^{13}F_{DIC.in}$ ($10^{-2}$ μmol/cm$^2$/yr) | $^{13}F_{DIC.out}$ ($10^{-2}$ μmol/cm$^2$/yr) | $F_{SO4.in}$ (μmol/cm$^2$/yr) | $F_{Ca}$ (μmol/cm$^2$/yr) | $^{13}C_{DIC-SMTZ}$ (‰) | $^{13}C_{CH4-SMTZ}$ (‰) | $^{13}C_{DIC-bot}$ (‰) | $^{13}C_{CH4-bot}$ (‰) | $\alpha_{CR}$ |
|---|---|---|---|---|---|---|---|---|---|---|---|
| **UBGH2-1_1** | 1.92 | 7.44 | 2.23 | 8.28 | -4.92 | -0.59 | -13.0 | -88.8 | 17.0 | -64.5 | 1.082 |
| **UBGH2-2_1** | 0.28 | 7.97 | 0.37 | 8.84 | -6.04 | -0.57 | -17.8 | -90.0 | 22.0 | -62.0 | 1.084 |
| **UBGH2-5** | 0.63 | 7.25 | 0.76 | 8.03 | -5.40 | -0.84 | -14.4 | -87.4 | 18.5 | -62.0 | 1.081 |
| **UBGH2-6** | 0.41 | 9.35 | 0.51 | 10.31 | -6.70 | -0.65 | -20.4 | -85.9 | 17.0 | -63.3 | 1.080 |
| **UBGH2-10** | 0.57 | 9.53 | 0.76 | 10.49 | -7.23 | -0.55 | -18.9 | -86.6 | 20.0 | -64.3 | 1.084 |

Table4
Click here to download Table: table4.pdf

Table 4 Error of flux estimates for each of the dissolved species considered in our model

| | UBGH2-1_1 | UBGH2-2_1 | UBGH2-5 | UBGH2-6 | UBGH2-10 |
|---|---|---|---|---|---|
| $F_{SO4}$ | 3.2% | 3.2% | 1.8% | 3.3% | 3.0% |
| $^{12}F_{DIC.in}$ | 6.2% | 14.7% | 20.3% | 9.1% | 12.6% |
| $^{12}F_{DIC.out}$ | 17.5% | 16.7% | 7.9% | 11.2% | 9.0% |
| $^{13}F_{DIC.in}$ | 6.3% | 8.9% | 20.2% | 9.1% | 11.8% |
| $^{13}F_{DIC.out}$ | 17.3% | 14.5% | 7.8% | 11.2% | 9.1% |
| $F_{Ca}$ | 3.2% | 4.9% | 12.0% | 4.4% | 2.9% |

Table5
Click here to download Table: table5.pdf

Table 5 Range of the depth-integrated reaction rates (μmol/cm$^2$/yr) derived from Case 4.

| | $R_{AOM}$ μmol/cm$^2$/yr | $R_{CR}$ μmol/cm$^2$/yr | $R_{CP}$ μmol/cm$^2$/yr | $R_{OM}$ μmol/cm$^2$/yr | $R_{ME}$ μmol/cm$^2$/yr | $R_{POCSR\text{-}C}$ μmol/cm$^2$/yr |
|---|---|---|---|---|---|---|
| **UBGH2-1_1** | 4.54±0.37 | 1.81±0.01 | 0.58 | 6.00±0.01 | 5.25±0.76 | 0.75±0.75 |
| **UBGH2-2_1** | 5.30±0.74 | 1.96±0.05 | 0.56 | 8.34±0.11 | 6.86±1.37 | 1.48±1.48 |
| **UBGH2-5** | 4.65±0.75 | 1.68±0.02 | 0.83 | 7.47±0.04 | 5.97±1.46 | 1.50±1.5 |
| **UBGH2-6** | 5.53±1.17 | 1.83±0.01 | 0.64 | 9.41±0.01 | 7.06±2.36 | 2.35±2.35 |
| **UBGH2-10** | 4.52±0.92 | 1.34±0.02 | 0.55 | 7.22±0.04 | 1.80±1.8 | 5.42±1.83 |

| Variables | Symbol | Value or Explanation |
|---|---|---|
| $\alpha$ | Degree of isotopic fractionation | |
| | $\alpha_{POCSR}$ | 1 |
| | $\alpha_{CP}$ | 1 |
| | $\alpha_{AMO}$ | 1.004-1.03 |
| | $\alpha_{ME}$ | 1.055-1.095 |
| | $\alpha_{CR}$ | 1.055-1.095 |
| b | Proportion of AMO that is being recycled through CR | |
| $\frac{\Delta(\phi C)}{\Delta z}$ | Concentration gradient (porosity corrected) | |
| $^{12/13}C$ | Concentration of carbon 12 or carbon 13 | |
| | $^{12/13}C_{CH4\text{-}SMTZ}$ | Concentration of carbon 12 or 13 of $CH_4$ at SMTZ |
| | $^{12/13}C_{CH4\text{-}bot}$ | Concentration of carbon 12 or 13 of $CH_4$ at the same depth as $r_{CH4\text{-}bot}$ |
| | $^{12/13}C_{DIC}$ | Concentration of carbon 12 or 13 of DIC |
| $\delta^{13}C$ | $\delta^{13}C_{CH2O}$ | Carbon isotope of organic matter |
| | $\delta^{13}C_{CH4\text{-}bot}$ | Carbon isotope of $CH_4$ at core bottom |
| | $\delta^{13}C_{CH4\text{-}SMTZ}$ | Carbon isotope of $CH_4$ at the SMTZ |
| | $\delta^{13}C_{DIC\text{-}bot}$ | Carbon isotope of DIC at core bottom |
| | $\delta^{13}C_{DIC\text{-}SMTZ}$ | Carbon isotope of DIC at the SMTZ |
| $C_T$ | Total concentration of carbon (*i.e.*, $^{12}C+^{13}C$) | |
| D | Diffusion coefficient | |
| f | Fraction of organic matter being utilized by POCSR | |
| $\phi$ | Porosity | |
| | $\phi_0$ | Porosity at water-sediment interface |
| | $\phi_f$ | Porosity at great depth |
| $F_{in}$ | Flux into SMTZ | |
| | $F_{SO4.in}$ | |
| | $F_{DIC.in}$ | |
| | $F_{CH4.in}$ | |
| | $F_{Ca}$ | |
| $F_{out}$ | Flux out from SMTZ | |
| | $F_{SO4.out}$ | |
| | $F_{DIC.out}$ | |
| | $F_{CH4.out}$ | |
| $\gamma$ | Empirical constant for porosity fitting | |
| k | Rate constant | |

| | | |
|---|---|---|
| | $k^L$ | Rate constant for light isotope |
| | $k^H$ | Rate constant for heavy isotope |
| r | $^{13}C/^{12}C$ ratio | |
| | $r_r$ | $^{13}C/^{12}C$ ratio of reactant |
| | $r_p$ | $^{13}C/^{12}C$ ratio of product |
| | $r_{std}$ | $^{13}C/^{12}C$ ratio of PDB standard (0.0112372) |
| | $r_{OM}$ | $^{13}C/^{12}C$ ratio of organic matter |
| | $r_{DIC}$ | $^{13}C/^{12}C$ ratio of DIC |
| | $r_{DIC\text{-}SMTZ}$ | $^{13}C/^{12}C$ ratio of DIC at SMTZ |
| | $r_{CH4\text{-}SMTZ}$ | $^{13}C/^{12}C$ ratio of $CH_4$ at SMTZ |
| | $r_{DIC\text{-}bot}$ | $^{13}C/^{12}C$ ratio of $CH_4$ at the depth where isotopic value approaching a fixed value |
| | $r_{CH4\text{-}bot}$ | $^{13}C/^{12}C$ ratio of $CH_4$ at the depth where isotopic value approaching a fixed value |
| $^{12/13}R$ | Reaction rate for carbon 12 or 13 | |
| | $^{12/13}R_{OM}$ | Gross organic matter degradation rate |
| | $^{12/13}R_{POCSR\text{-}S}$ | Rate of POC sulfate reduction in terms of sulfate consumption |
| | $^{12/13}R_{POCSR\text{-}C}$ | Rate of POC sulfate reduction in terms of DIC production |
| | $^{12/13}R_{CP}$ | Rate of carbonate precipitation |
| | $^{12/13}R_{AOM}$ | Rate of anaerobic oxidation of methane |
| | $^{12/13}R_{ME\text{-}CH4}$ | Rate methane production from methanogenesis |
| | $^{12/13}R_{ME\text{-}DIC}$ | Rate DIC production from methanogenesis |
| | $^{12/13}R_{CR}$ | Rate of $CO_2$ reduction |
| z | Depth in the sediments | |

Electronic Supplementary Material

Click here to download Electronic Supplementary Material: Hong_etal_boxmodel.xls